Experimental Section

Autoclaves were loaded with reactants in a glove box (Saffron) under N_2. IR spectra were recorded on a Perkin-Elmer 100 spectrometer with universal ATR. Elemental analysis was obtained using a Perkin-Elmer 4200 elemental analyser. Powder X-ray diffraction (XRD) experiments were performed using a X'Pert Pro diffractometer with Cu-Kα radiation (λ= 1.5418Å) operating at 40 kV and 40 mA and the scanning angle ranged from 10° to 90° of 2θ. Both carbon and hydrogen analyses were done using a vario Micro Elemental analyzer (Elementar Analysensysteme GmbH, Germany). Nuclear magnetic resonance (NMR) spectra in solution were recorded on a Bruker Avance III 500-MHz spectrometer at 298 K using chloroform-d ($CDCl_3$) as solvent and tetramethylsilane as standard. Scanning electron microscopy (SEM) images were collected using a field emission scanning electron microscope (Hitachi S-4800). Transmission electron microscopy (TEM) was performed with a FEI Tecnai G2 F30 electron microscope operating at an accelerating voltage of 300 kV. The surface compositions of sample **A** and **B** were determined by energy dispersive spectroscopy (EDS). EDS data were collected using an Thermo SCIENTIFIC energy dispersive X-ray spectroscopy system attached to a Hitachi S-4800 SEM, with an acceleration voltage of 15keV. X-ray photoelectron spectra (XPS) were operated on a spectrometer (Kratos AXIS Ultra DLD, Shimadzu, Japan). Thermogravimetric analysis was obtained using a TA Q100-DSC thermal analyzer, with a constant heating rate of 5 ^oC/min in air atmosphere. UV-visible spectra of powdered samples of **A** and **B** were recorded in diffuse reflectance mode using a Perkin Elmer Lambda 12 UV-visible spectrometer equipped with an integration sphere (Labsphere RSA-PE-20) and referenced to a white PTFE standard.

*Synthesis and Characterisation of **1***

Titanium ethoxide (> 97% Sigma-Aldrich, 2 ml, 8.8 mmol), $EuCl_3$ (99% Sigma-Aldrich, 0.258g, 1mmol) and anhydrous ethanol (Sigma-Aldrich, 5.0ml) were mixed in a Teflon-lined autoclave and heated at 150^oC for 3 days. Slow cooling to room temperature gave a colourless solution. Clourless block crystals of **4** were obtained by slow evaporation of the filtered solution at room temperature for four weeks, Yield 0.15g (21.2 % with respect to Eu supplied). 1H NMR (500.1 MHz, +25$^oCDCl_3$, δ ppm), collection of multiplets in the ranges 5.0-3.4 (CH_2-O) and 2.0-0.8 (CH_3). Elemental analysis; found C 31.2, H 6.8, Cl 4.9; cald. for **1**, C 30.6, H. 6.6, Cl 5.0. IR (800-4000 cm^{-1}), ν/ cm^{-1} = 891(m), 924(m), 1043(vs), 1091(s), 1123(s), 1376(m), 1440(w), 2359(w), 2866(m), 2925(m), 2969 (m), 3323(w).

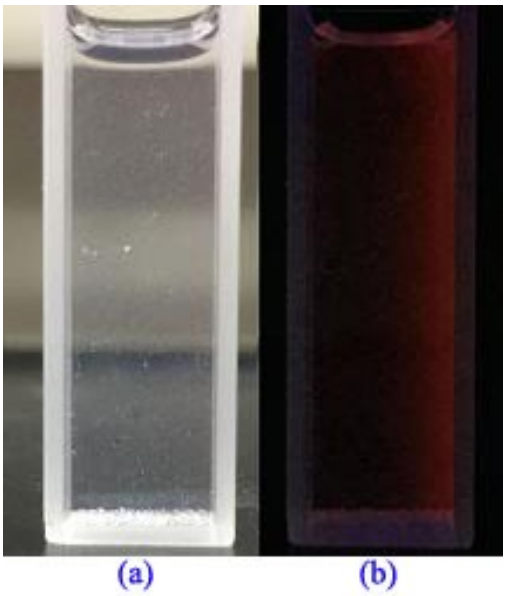

Fig. S1 (a) Optical image of dichloromethane solution of **1**, **(b)** image of the fluorescence emission of dichloromethane solution of **1** under 254 nm irradiation.

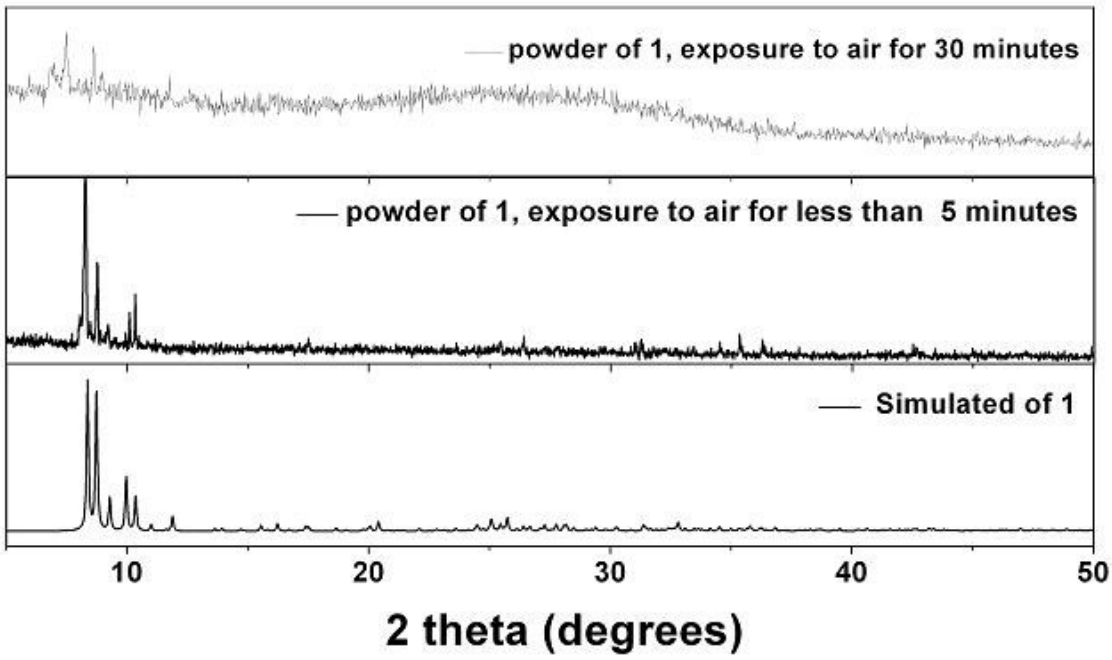

Fig. S2 Powder-XRD results of cage **1 .**

As shown in **Fig. S2**, the simulated XRD patterns of cage**1** coincide well with the measured powder XRD patterns.The diffraction peaks at 2θ= 8.34°, 8.34°, 9.30°, 9.92° and 10.36° can be indexed to (0,1,1), (1,1,0), (0,2,0), (1,0,-1) and (1,0,1) crystal planes of **1**. However, most diffraction peaks were disappeared after exposed to air for 30 minutes, which indicated the sample had been hydrolyzed and decomposed.

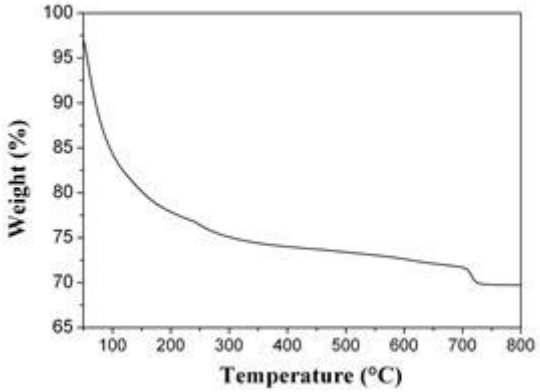

Fig. S3 TG curve of cage **1**

Single Crystal X-ray Crystallography

Crystal data were collected on a Bruker Smart Apex CCD diffractometer. The structures were solved by Direct Methods and refined by full-matrix least squares on F^2. (Ref: SHELX, G. M. Sheldrick, *Acta Crystallogr.* **2008**, *A64*, 112).

Table SI-1 Details of the structure solution and refinement of **1**

Compound	**8**
Chemical formula	$C_{36}H_{92}Cl_2Eu_2O_{20}Ti_4$
FW	1411.52
Crystal system	Monoclinic
Space group	*P* 21/n
Unit cell dimensions	
a (Å)	11.9475(7)
b (Å)	18.9968(13)
c (Å)	12.7731(9)
α (°)	
β (°)	92.489(2)
γ (°)	
V (Å^3)	2896.3(3)
Z	2
ρ_{calc} (Mg/m^3)	1.619
μ (Mo-Kα) (mm^{-1})	2.812
reflections collected	26482
independent reflections (R_{int})	5091 (0.0237)
*R*1, *wR*2 [$I>2\sigma(I)$]	0.0230 0.0615
*R*1, *wR*2 (all data)	0.0257 0.0636

Table SI-2 Selected bond lengths (Å) and angles (°).

Bond	Distance	Bond	Distance
Eu1–O2#1	2.3691(19)	Eu1–O3	2.4557(19)
Eu1–O2	2.3777(18)	Eu1–O10#1	2.466(2)
Eu1–O1	2.439(2)	Eu1–O4	2.5749(19)
Eu1–O6	2.454(2)	Eu1–Cl1	2.6838(8)
Ti1–O8	1.789(2)	Ti2–O9	1.790(2)
Ti1–O7	1.861(2)	Ti2–O10	1.919(2)
Ti1–O3	1.936(2)	Ti2–O6	1.922(2)
Ti1–O2	1.9808(19)	Ti2–O2	2.0079(19)
Ti1–O5	2.071(2)	Ti2–O5	2.023(2)
Ti1–O4	2.168(2)	Ti2–O4	2.115(2)
O2#1–Eu1–O2	74.06(7)	O3–Eu1–O10#1	80.85(7)
O2#1–Eu1–O1	75.28(7)	O2#1–Eu1–O4	126.09(6)
O2–Eu1–O1	137.81(7)	O2–Eu1–O4	58.15(6)

O2#1–Eu1–O6	78.28(6)	O1–Eu1–O4	125.28(7)
O2–Eu1–O6	67.57(6)	O6–Eu1–O4	62.24(6)
O1–Eu1–O6	78.39(7)	O3–Eu1–O4	65.59(6)
O2#1–Eu1–O3	116.41(7)	O10#1–Eu1–O4	146.28(7)
O2–Eu1–O3	64.79(6)	O2#1–Eu1–Cl1	145.92(5)
O1–Eu1–O3	157.06(7)	O2–Eu1–Cl1	139.36(5)
O6–Eu1–O3	122.13(6)	O1–Eu1–Cl1	77.79(5)
O2#1–Eu1–O10#1	65.61(6)	O6–Eu1–Cl1	116.15(5)
O2–Eu1–O10#1	105.38(7)	O3–Eu1–Cl1	83.25(5)
O1–Eu1–O10#1	87.25(8)	O10#1–Eu1–Cl1	92.77(5)
O6–Eu1–O10#1	143.51(7)	O4–Eu1–Cl1	86.73(5)

Symmetry code: (#1) 1–*x*, –*y*, –*z*.

*Preparation of **A***, ***B***, and ***P***

20ml dichloromethane solution of **1** (0.1 mmol) was dissolved in 60ml 50% ethanol aqueous solution and then stirred under ultrasound. After filtering the suspension and drying at 150 °C for 12h, a white powder of **A** was obtained.

1.5g of dried crystals of **1** was heated at 500 °C for 5 hour in a (dry) air flow, an off-white solid of **B** was obtained.

Precursor **1** was dissolved in poly-methylmethacrylate (weight ratio 1:20) in a toluene-dichloromethane mixed solution. The resulting solution was cast onto a clean glass plate and dried at 15 °C. Film **P** were obtained by soaking the glass plates in de-ionized water which led to the films separating from the glass substrate.

*Elemental Analysis of **A*** and ***B***

A, C 0.51 wt %, H 0.72%; **B**, C 1.12 wt %, H 0.44%. These results can be compared to EDS measurements which show much higher C and H values due to background and surface contamination.

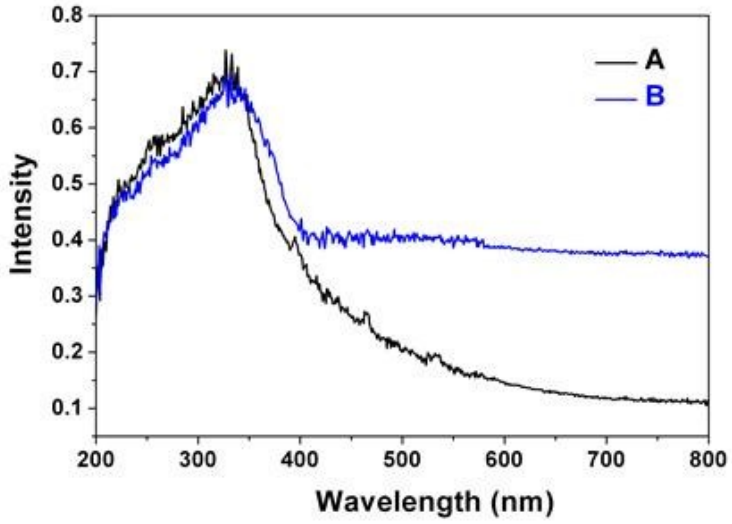

Fig. S4 Solid-state UV-vis absorption spectra of **A** and **B**

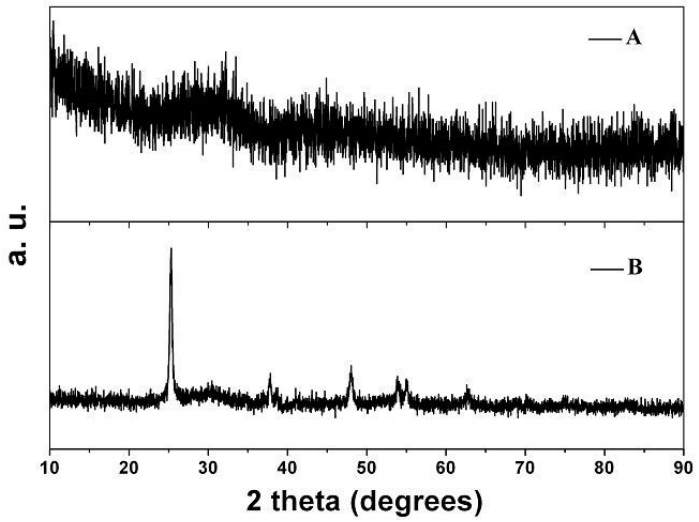

Fig. S5 Powder-XRD of **A** and **B**

The *p*XRD result for sample **B** show that the TiO_2 is present in the form of anatase and there is a weak peak at 30.35 degree which is contributed by $Eu_2Ti_2O_7$; whereas **A** is amorphous. (Ref: J. L. Her, C. W. Lin, K. Y. Chang and T. M. Pan, *Int. J. Electrochem. Sci*., 2012, **7**, 387-404).

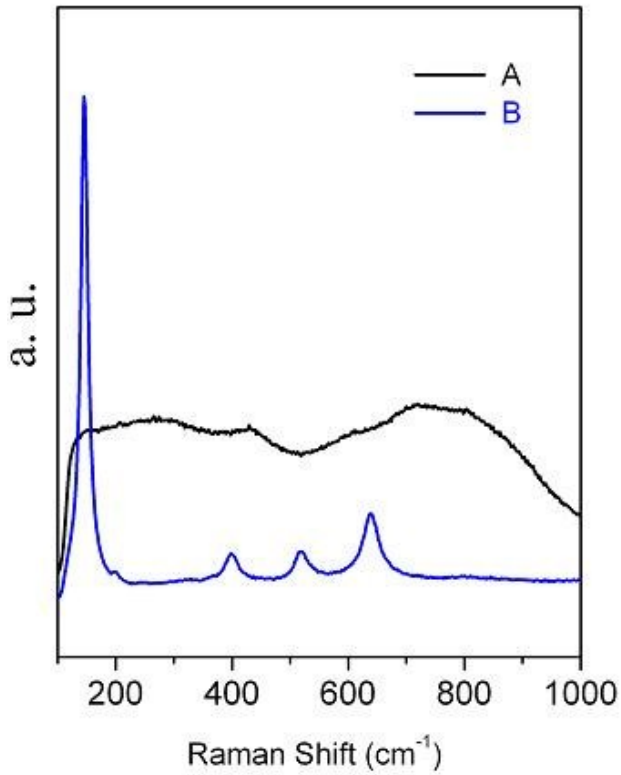

Fig. S6 Raman spectra of **A** and **B**

Raman spectra of sample **A** exhibit several broad bands centered at 275, 432, 606, 720, 805cm^{-1} due to its amorphous phase, but raman spectra of sample **B** show sharp peaks at 145, 199, 399, 519, 642 cm^{-1} which is contributed by anatase phase (Ref: O. Frank, M. Zukalova, B. Laskova, J. Kürti, J. Koltai and L. Kavan, *Phys. Chem. Chem. Phys*., 2012, **14**, 14567-14572).

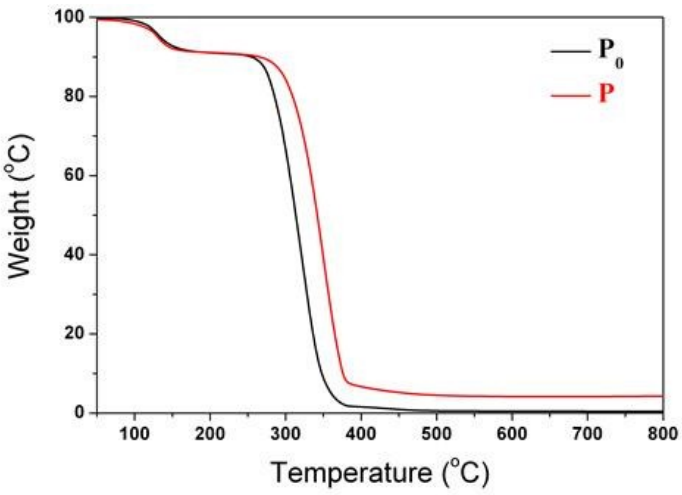

Fig. S7 TG curve of $\mathbf{P_0}$ and **P**.

The thermal stability of the films is evaluated by the 10% weight loss temperatures ($T_{10\%}$). As shown in Fig. S5, both $\mathbf{P_0}$ and **P** are stable up to 250 °C, $T_{10\%}$ of **P** is 265.4 °C [higher than that of $\mathbf{P_0}$ (254.8 °C)]. It can be seen that the thermal stability of the PMMA film is increased after incorporation of cage **1**.

*Adjustment of film **P**.*

Changing the weight ratio of cage **1** and poly-methylmethacrylate into 1:10 ($\boldsymbol{P_1}$) and 1:5 ($\boldsymbol{P_2}$), we can obtain different films show stronger fluorescence (Fig S8), the emission intensity increases with the increase of concentration of **1**; altering the drying temperature from 15°C to 40 °C, the surface of **P** can be adjusted from smooth to porous (Fig S9b, Fig S9c). Moreover, the thickness of film P can also be adjusted (Fig S9).

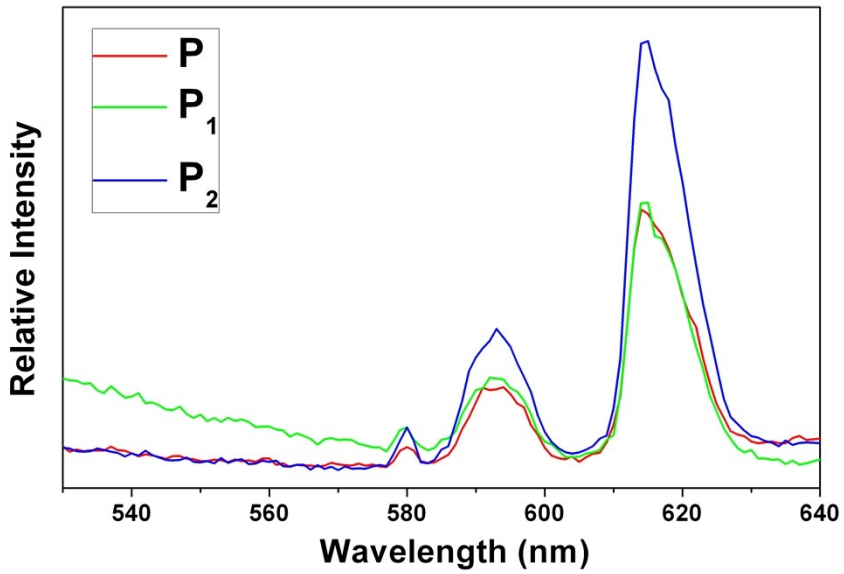

Fig. S8 emission spectra of $\mathbf{P_1}$, $\mathbf{P_2}$ and **P** under 326 nm excitation.

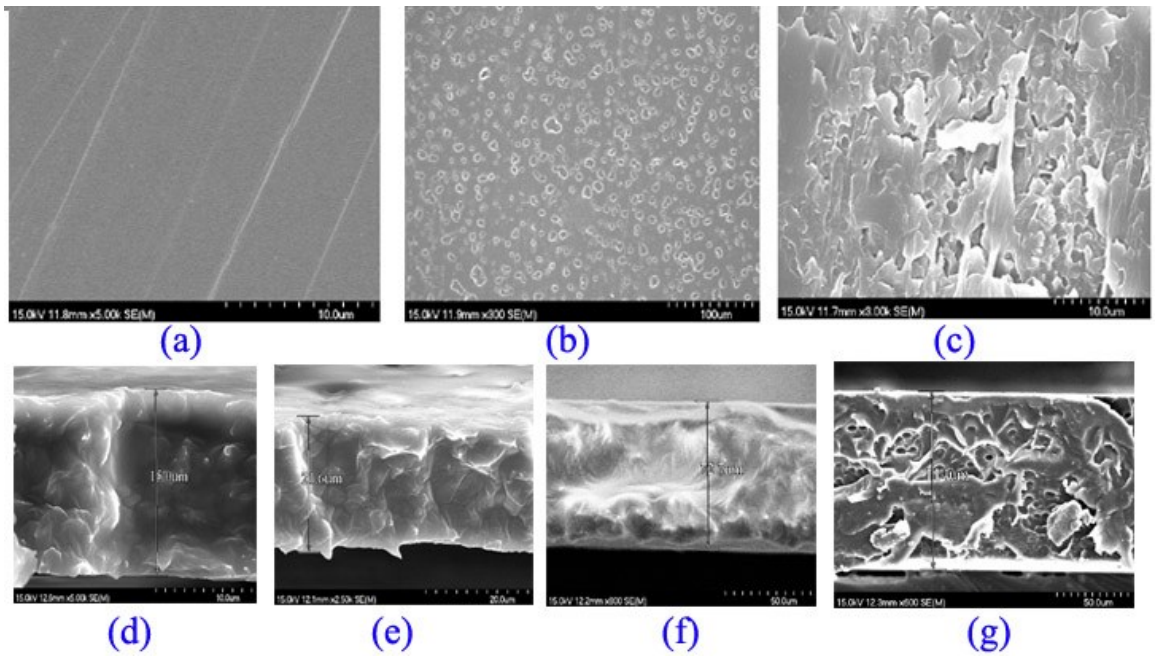

Fig. S9 SEM images of films **P** with (a) smooth surface, (b) porous surface and (c) surface defects; SEM images of cross-section of films **P** with (d) 15μm, (e) 21.6μm, (f) 72.7μm, (g) 114μm.

*EDS Analysis of **A** and **B***

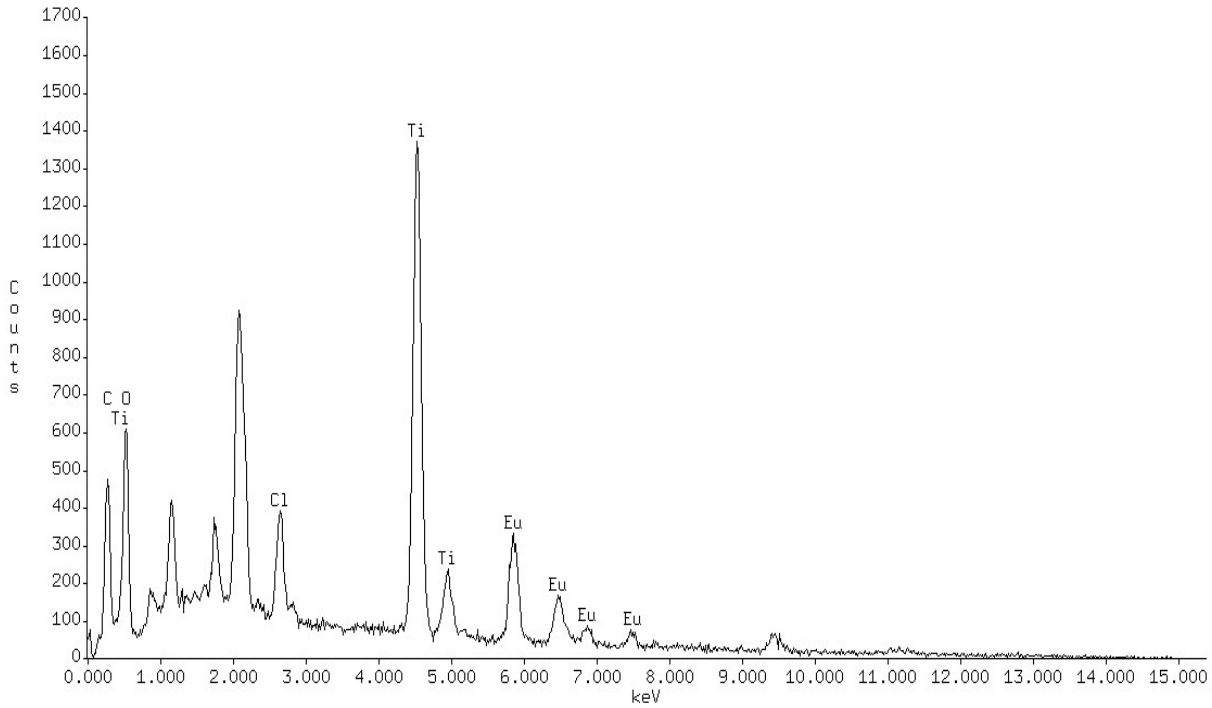

Fig. S10 EDS on sample **A**

Table S3 EDS on sample **A**

Element	Atomic Percentage	Weight Percentage
C	33.28 %	15.05 %
O	44.82 %	27.00 %
Cl	2.13 %	2.85 %
Ti	14.81 %	26.71 %
Eu	4.96 %	28.39 %

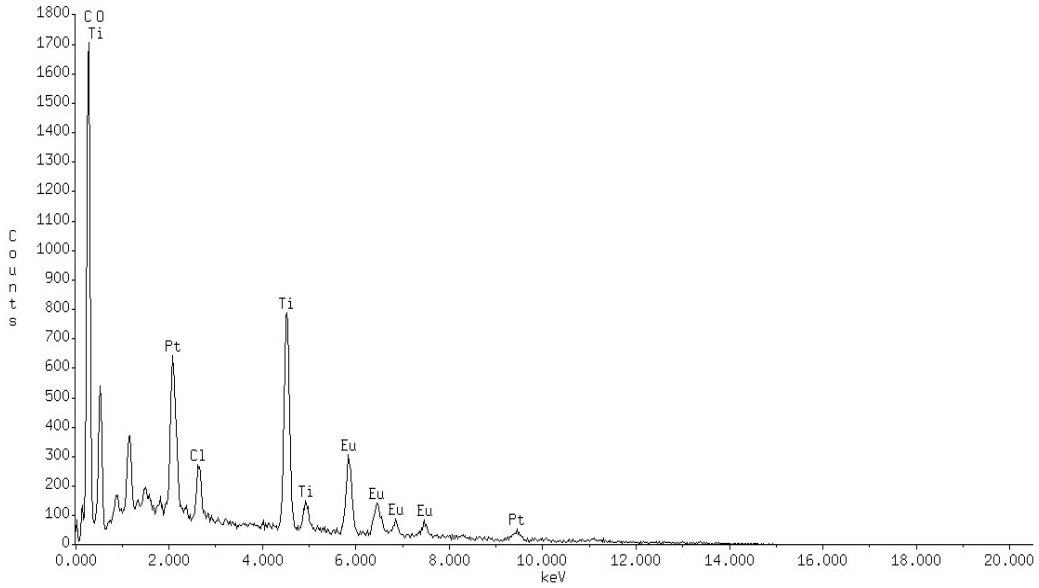

Fig. S11 EDS on sample **B**

Table S3 EDS on sample **B**

Element	Atomic Percentage	Weight Percentage
C	31.51 %	11.63 %
O	40.24 %	19.78 %
Cl	1.18 %	1.28 %
Ti	12.91 %	19.01 %
Eu	7.60 %	35.52 %

*XPS Analysis of **A** and **B***

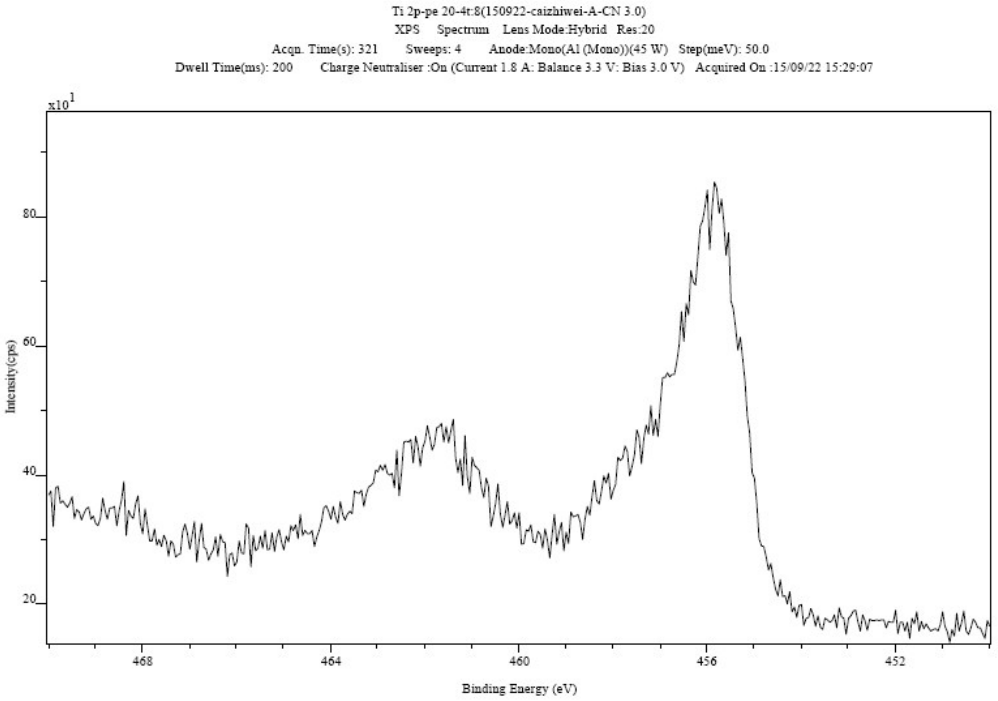

Fig. S12 XPS signal of **A** for Ti *2p* region.

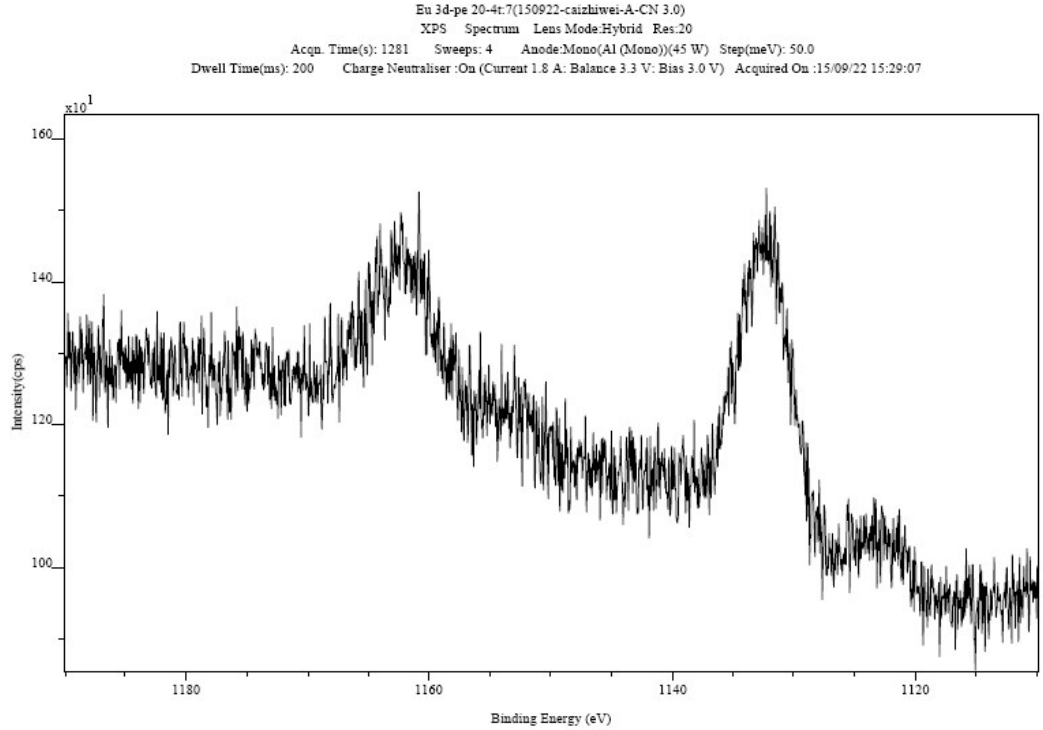

Fig. S13 XPS signal of **A** for Eu 3*d* region

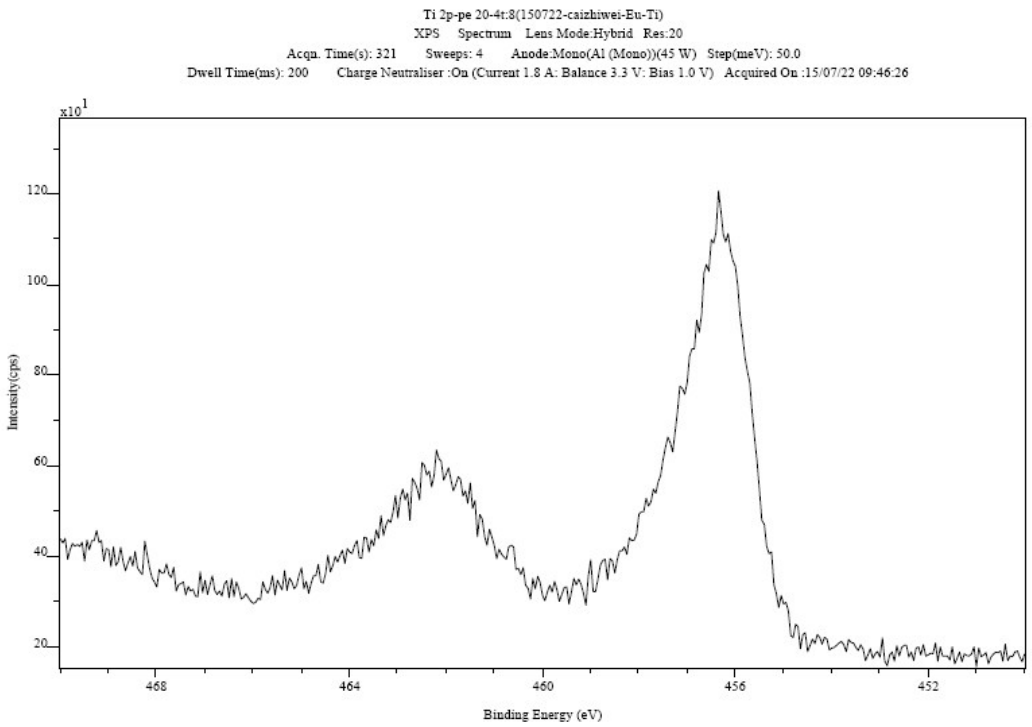

Fig. S14 XPS signal of **B** for Ti *2p* region.

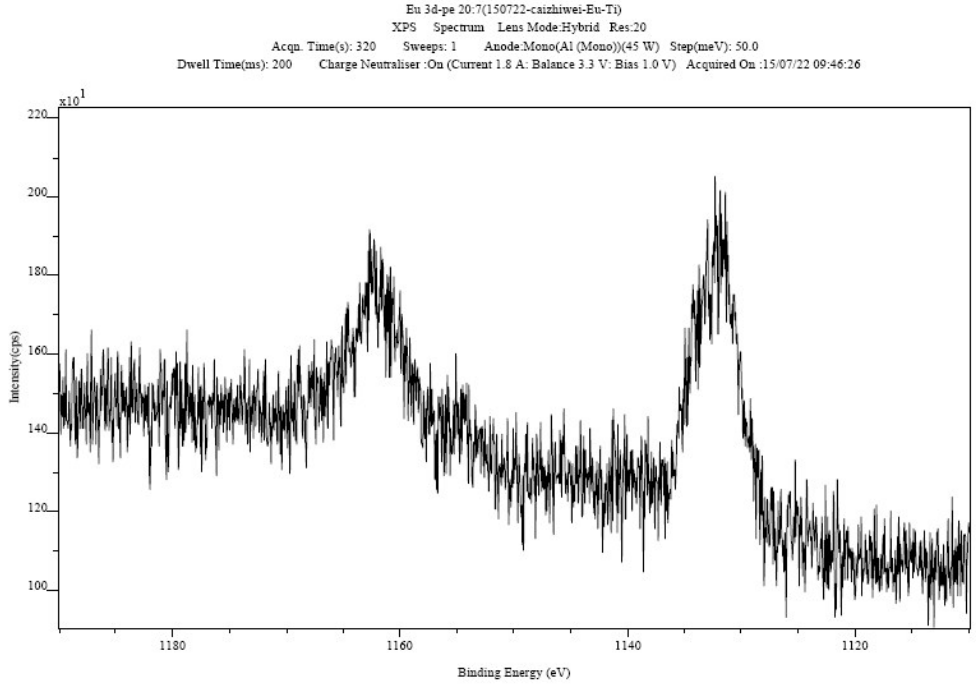

Fig. S15 XPS signal of **B** for Eu 3*d* region

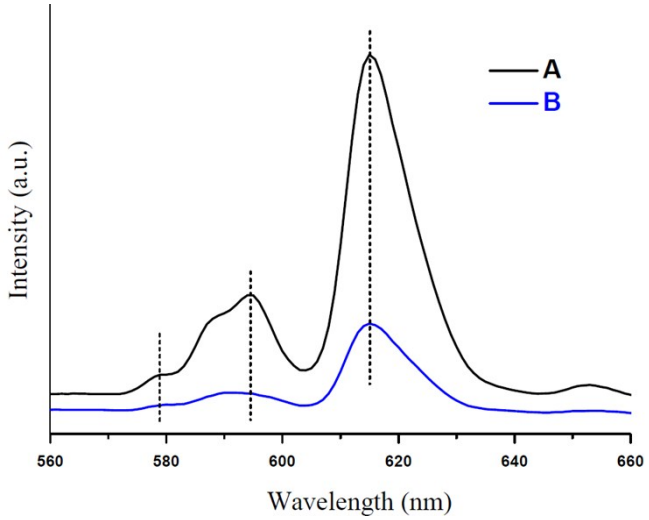

Fig. S16 fluorescence spectrum of A and B under 365 nm excitation

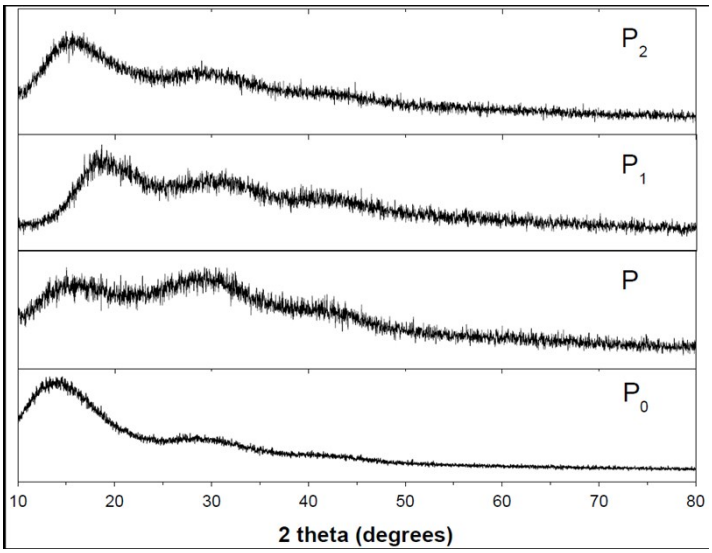

Fig. S17 Powder-XRD of $\mathbf{P_0}$, **P**, $\mathbf{P_1}$ and $\mathbf{P_2}$.

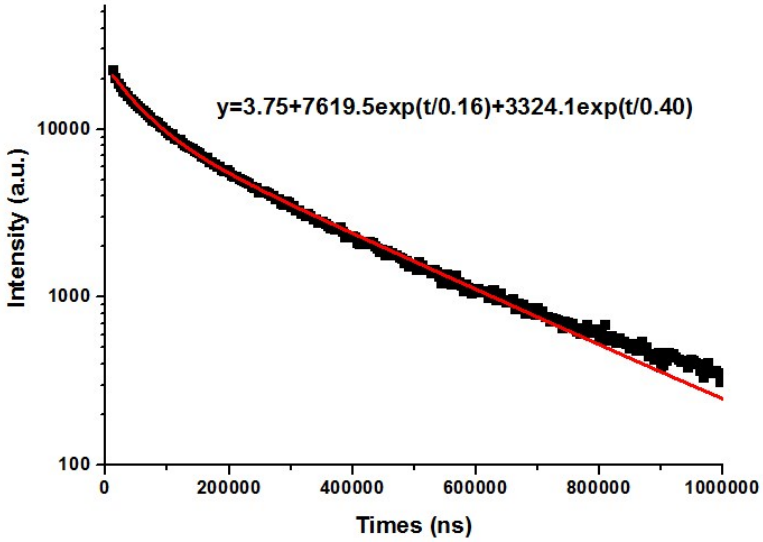

Figure **S18**. The decay and fitting curves of PL lifetime spectrum.